

See discussions, stats, and author profiles for this publication at: <https://www.researchgate.net/publication/51662752>

Scaling of Excitons in Graphene Nanoribbons with Armchair Shaped Edges

ARTICLE *in* THE JOURNAL OF PHYSICAL CHEMISTRY A · SEPTEMBER 2011

Impact Factor: 2.69 · DOI: 10.1021/jp202787h · Source: PubMed

CITATIONS

19

READS

69

2 AUTHORS, INCLUDING:




Haibin Su

Nanyang Technological University

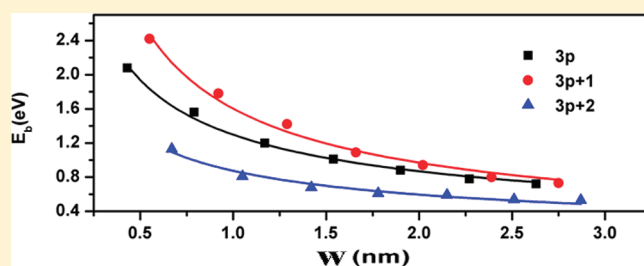
174 PUBLICATIONS 2,096 CITATIONS

SEE PROFILE

Scaling of Excitons in Graphene Nanoribbons with Armchair Shaped Edges

Xi Zhu[†] and Haibin Su^{*,†,‡,§}[†]Division of Materials Science, Nanyang Technological University, 50 Nanyang Avenue, Singapore 639798, Singapore[‡]Institute of Advanced Studies, Nanyang Technological University, 60 Nanyang View, Singapore 639673, Singapore[§]Institute of High Performance Computing, 1 Fusionopolis Way, Connexis 138632, Singapore Supporting Information

ABSTRACT: The scaling behavior of band gaps and fundamental quantities of exciton, i.e., reduced mass, size, and binding strength, in three families of quasi one-dimensional graphene nanoribbons with hydrogen passivated armchair shaped edge (AGNRs) are comprehensively investigated by density functional theory with quasi-particle corrections and many body, i.e., electron–hole, interactions. Compared with single-walled carbon nanotubes (SWCNTs) where the scaling character features a single exponent, each family of AGNRs has its own single exponent, due to its intrinsic zero curvature, which also accounts for the absent “family spreading” of optical transition energies in the smaller width region in the Kataura plots of AGNRs as compared to those of SWCNTs. Moreover, the scaling relation between exciton binding strength and the geometric parameter is established.



INTRODUCTION

Graphene, a single aromatic plane of sp^2 bonded carbon in a hexagonal lattice, comes closer to the two-dimensional system ideal than do the semiconductor electron gases,^{1–3} manifested by the remarkable electronic properties, such as integer and the fractional quantum Hall effect in particular.^{4–7} Owing to its flat structure as compared to the cylindrical shape of carbon nanotubes, graphene is a better fit to semiconductor architecture and more compatible with the fabrication technology. Among a string of discoveries that include new fundamental insights and promising schemes to turn them into novel devices driven by the impetus for the post CMOS electronics revolution, one milestone is the success of graphene transistors, enabled by the superior carrier mobility, that can operate at 100 GHz about 10 times as fast as the speediest silicon transistors.⁸ Moreover, worldwide intensive efforts have also been input to investigate the spatially confined elongated strips of graphene bounded by straight edges, termed graphene nanoribbons (GNRs), which are predicted to be semiconducting due to edge effects and quantum confinement of the electron wave function in the transverse direction.^{9–12} The semiconducting character of sub-10-nm GNRs can be ready for the needs of post CMOS semiconductor devices. However, it is experimentally challenging to fabricate GNRs in the sub-10-nm regime. The e-beam lithography approach is usually limited by a line edge roughness of 1–3 nm of GNRs, which can adversely impact their electronic properties and make it practically impossible to obtain GNRs in the sub-5-nm regime.^{13,14} Two significant breakthroughs have been

made recently to demonstrate that GNRs with ultranarrow width down to 2–3 nm with smooth edges can be produced from the unzipping carbon nanotubes through plasma etching and solution-based oxidation processes.^{15,16} Interestingly, one rational approach is reported to fabricate sub-10-nm GNRs in the oxygen plasma etch process using chemically synthesized nanowires with controllable sizes down to 1 nm with a nearly atomically smooth line edge as etch mask.¹⁷ Significantly, room temperature FETs have been demonstrated from all these ultranarrow GNRs. All these studies advance the GNR based electronics remarkably.

The emission spectrum of carbon nanotubes dominated by excitonic recombination is firmly established through intensive studies on the optical properties of single-walled carbon nanotubes (SWCNTs) with high resolution measurements and many-body theoretical approaches.^{18–20} The observed strong family dependent excitonic effect originates from the quasi 1D structure of SWCNT.^{21,22} Particularly, the explicit scaling behavior is thoroughly studied by Perebeinos et al.²³ including a series of simple linear scaling formulas between the exciton binding energy, the SWCNTs' sizes and dielectric environments (dielectric constants), and the oscillation strength.²³ Considering that semiconductor GNRs are direct-band gap materials as well, it is intriguing to explore the optical properties of GNRs for

Received: March 25, 2011

Revised: August 31, 2011

Published: September 22, 2011

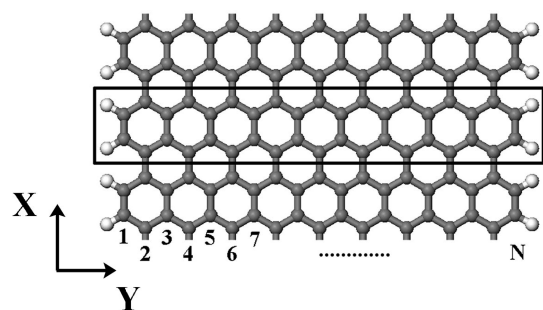


Figure 1. Schematic of typical AGNRs passivated by hydrogen atoms in the edges. Hydrogen and carbon atoms are represented by white and gray colors, respectively. The AGNRs are periodic in the X direction.

building integrated electronic and optoelectronic devices to generate and detect light.

In this work, we perform first-principles calculations to study the scaling law of the excitonic properties for different widths of graphene nanoribbons with armchair shape edges (AGNRs). First, we introduce the method used for studying electronic and optical properties. Then, we investigate the feature of the Kataura plot of AGNRs and the family dependent exciton wave function size. Finally, we establish a set of scaling formulas to correlate the width of the AGNRs with the exciton binding energy, size of exciton wave function, and the reduced mass.

METHODOLOGY

The first-principles calculation of the optical excitations is carried out using a many-body perturbation theory approach, based on a three-step procedure.²⁴ First we obtain the ground-state electronic properties of the relaxed system within the local density approximation (LDA) using *Quantum ESPRESSO*²⁵ code. The calculations are carried out using separable normconserving pseudopotentials and a plane-wave basis set with the kinetic energy cutoff of 30 Ry and 71 *k*-points. Each atomic structure is fully relaxed, until forces acting on atoms are less than 0.01 eV/Å. Next, the quasiparticle corrections to the LDA eigenvalues are computed within the G0W0 approximation for the self-energy operator, where the LDA wave functions are used as good approximations for the quasiparticle ones, and the screening is treated within the plasmon-pole approximation.²⁶ The electron–hole interaction is included by solving the Bethe–Salpeter equation (BSE) in the basis set of quasi electron and quasi hole states, where the static screening in the direct term is calculated within the random-phase approximation²⁷

$$(E_{ck} - E_{vk})A_{vck}^S + \sum_{k'v'c'} \langle vck | K^{eh} | v'c'k' \rangle A_{v'c'k'}^S = \Omega^S A_{vck}^S \quad (1)$$

where A_{vck}^S is the exciton wave function, K^{eh} is the electron–hole coupling kernel, Ω^S is the excitation energy, and E_{ck} and E_{vk} are the quasiparticle energy of the electron and hole states respectively. Because the supercell method is used in these calculations, a rectangular-shape truncated Coulomb interaction is applied to eliminate the image effect between adjacent supercells to mimic isolated GNRs.^{10,28,29} We use total 10 valence bands and 10 conduction bands with the Fermi level lies in between in our BSE calculation. All the GW–BS calculations are performed with the Yambo code³⁰ for light polarized along the ribbon principal axis, i.e., X-axis shown in Figure 1, to avoid significant quenching due to the depolarization effect for the perpendicular

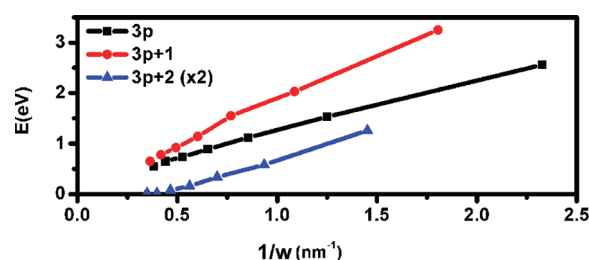


Figure 2. Kataura plot of AGNRs. The transition energy of the $3p+2$ family is doubled for clarify. The “family spreading” in the smaller width region is absent due to the intrinsic zero curvature of AGNRs.

polarization.^{31,32} For the same structures, the results shown in Table S1 (see Supporting Information for details) of this work are in accord with the previous study.^{33–35}

RESULTS AND DISCUSSION

The AGNRs can be categorized into three families depending on their width by $N = 3p, 3p+1, 3p+2$ (p is an integer), the width of the nanoribbon, N , is defined as in Figure 1. The dependence of band gap, optical transition energy, and the exciton’s binding energy on the width of AGNRs is shown in Table SI (see Supporting Information for details). The delicate family effect on gaps is that the gaps of these three families with the same p follow the following order: $E_g(3p+1) > E_g(3p) > E_g(3p+2)$, which is in good agreement with the previous studies.^{9–11} Within each family of AGNRs, the gap reduces with increased width by a power law. The exponents are -0.80 (for $3p$), -0.99 (for $3p+1$), and -1.54 (for $3p+2$) (see the Supporting Information). It is interesting to note that the general trend discussed above remains valid after including self-energy by the quasi-particle GW scheme. As shown in Table S1 (Supporting Information), the so-called “scissors operator”, in which the self-energy is approximated by a rigid shift of energy bands, clearly cannot be applied legitimately here due to the complicated band and energy dependence of GW corrections.^{9,10} Particularly, the GW corrections, i.e. the self-energy, in energy gaps of $3p$ and $3p+1$ families are larger than those of $3p+2$. In addition, the self-energy of same family of AGNRs with larger LDA gaps is larger. Note that the GW energy corrections on the order of 1 eV are somewhat larger than those found for bulk graphite or diamond due to the ineffective screening for reduced dimensions.³⁶

The Kataura plot, which is widely used in analyzing resonance Raman scattering and photoluminescence spectroscopy, correlates the optical transition energies and the diameters of SWCNTs.³⁷ Moreover, the transition energies are categorized by three family bands on the basis of the chirality of SWCNTs in the Kataura plot.³⁷ Thus, it is natural to examine the optical transition energies of AGNRs by the Kataura plot. The optical transition energies are computed by solving BSE numerically. Note that the screening in one and quasi-one-dimensional materials is orders of magnitude weaker than in bulk materials. The free electron screening in the former case diverges logarithmically rather than in a power-law manner in the bulk metallic materials.^{38,39} The absolute values of optical transition energies, as tabulated in Table SI (Supporting Information), are about half (a much smaller fraction) of GW gap values for the $3p$ and $3p+1$ ($3p+2$) families, which is the clear manifestation of strong coupling of the electron and hole in AGNRs. Interestingly, the family pattern can be clearly observed in the Kataura plot for

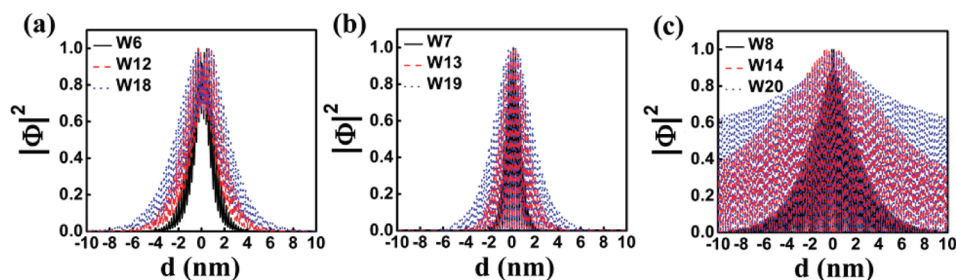


Figure 3. Exciton wave function along the principal axis of three families of AGNRs: $3p$ (A), $3p+1$ (B), and $3p+2$ (C). The X-axis shows the distance (d) with respect to the center of the exciton, which is set as the origin. Three structures in each family are chosen: W6, W12, W18 for the $3p$ family, W7, W13, W19 for the $3p+1$ family, and W8, W14, W20 for the $3p+2$ family.

AGNRs as shown in Figure 2. For the AGNRs with the same p , the optical transition energy is the largest for $3p+1$, followed by $3p$'s, and $3p+2$'s being the smallest. However, there is one fundamental difference in terms of the spread within a family of SWNTs and AGNRs in the Kataura plot. It is well-known that notable spread in the smaller diameter region of a family of SWNTs is largely attributed to the curvature effect, which leads to the hybridization of the π^* and σ^* orbitals of carbon.^{20,40} As shown in Figure 2, the trend of optical transition energy has linear character within a family of AGNRs. The “family spreading” in smaller width region is clearly absent due to its intrinsic zero curvature.

To gain insight of electron–hole interaction, we examine the wave function of excitons, $\Psi(\vec{r}_e, \vec{r}_h)$, with the lowest excitation energy in real space with one fixed hole position for all the AGNR studied in this work. The general patterns of exciton wave functions are very alike within the same family. This main feature in spatial distribution can be understood by performing the direct product of wave functions of the top valence band and bottom conduction band at the Γ point. The projections of the exciton wave functions along the width of AGNRs are presented in Figure 3a–c. The size of the wave function of each family grows as the AGNRs width increases. In particular, for the $3p+2$ family, the exciton's size expands rapidly with increased width, whereas the exciton size of the $3p+1$ and $3p$ family increases relatively modestly. Because the exciton wave function, $\Psi(\vec{r}_e, \vec{r}_h)$, is not limited within interatomic distance, it clearly has a non-Frenkel feature along the AGNR X-axis^{20,22} and is determined by the weakly screened Coulomb interaction associated with one-dimensional character in the AGNRs. The exciton binding energy is defined as the difference between the GW gap and optical transition energies. In general, the electron–hole interaction kernel has an attractive direct term by the screened Coulomb interaction and a repulsive exchange term mediated by the bare Coulomb interaction.²⁷ Thus, the exciton binding strength in AGNRs is expected to be strong, which is indeed consistent with the order of electronvolts, as shown in Table S1 (Supporting Information). For the AGNRs with the same p value, the GW corrected gaps of three families decrease from $3p+1$, to $3p$, then to $3p+2$, which results in a significantly heavier effective mass and fairly weaker screening to reduce the Coulomb interaction between the electron and hole for $3p+1$ and $3p$ compared with the case for $3p+2$. Therefore, exciton binding energies of the $3p+1$ and $3p$ families are much stronger than that of $3p+2$. The exciton binding energy approaches tens of millielectronvolts in the $3p+2$ family.

One scaling law between the exciton binding energy (E_b) with the radius (R), dielectric constant (ϵ), and effective mass (m) in SWCNTs has been proposed by using one dimensionless function to express the exciton size,²³

$$E_b = A_b R^{\alpha-2} m^{\alpha-1} \epsilon^{-\alpha} \quad (2)$$

where A_b and α are parameters obtained by fitting. This general scaling relationship is very useful for describing exciton binding strength as a function of their diameter and the dielectric constant of the environment in SWCNTs. However, the linear scaling of the exciton size (L) with the width (w) of AGNR does not hold for the AGNRs. In this study, the following power law relationship is proposed

$$L = A w^{\xi} \quad (3)$$

where A and ξ are parameters for fitting. The scaling of the size of the wave function (L) and the width of the ANGRs (W) are also presented in Figure 4a–c. Each family has its own index: 0.6 (for $3p$), 0.8 (for $3p+1$), and 0.3 (for $3p+2$), respectively. Here we propose one scaling law for the exciton in AGNRs using eq 3:

$$E_b = A_f w^{(\alpha-2)\xi} m^{\alpha-1} \epsilon^{-\alpha} \quad (4)$$

where A_f is a coefficient and ξ and α are the exponents defined in eqs 2 and 3, respectively. As shown in Figure 4, eq 4 captures the generic scaling features for all AGNRs studied in this work. The values of α are 0.98 (for $3p$), 1.0 (for $3p+1$), and 1.16 (for $3p+2$), respectively, which clearly deviate from 1.4 obtained by fitting SWCNT data with eq 2.²³ This results from the different effects of the GNR's width as compared to the CNT's diameter on exciton size and the effects of the family dependent effective mass. Considering that the value of α in bulk semiconductors is equal to 2, the much smaller value of α in both GNR and CNT shows the dramatic weak screening resulting from low-dimensional systems. Particularly, the smaller α values in AGNRs lead to much less influence of dielectric media on the exciton binding strength.

Now we analyze the reduced mass, which is defined as $m_e m_h / (m_e + m_h)$ in the unit m_0 (the mass of free electron). Note that the warping effect on the mass of AGNRs with the same p yields $m(3p+1) > m(3p) > m(3p+2)$. We start with the observation of power law relationship between the reduced mass and width of each family of AGNR

$$m = A_t w^{\tau} \quad (5)$$

where A_t and τ are family dependent parameters. The raw data and fitted curves are presented in Figure 5, and the values of τ are listed in Table 1. Generally, the reduced mass decreases as the

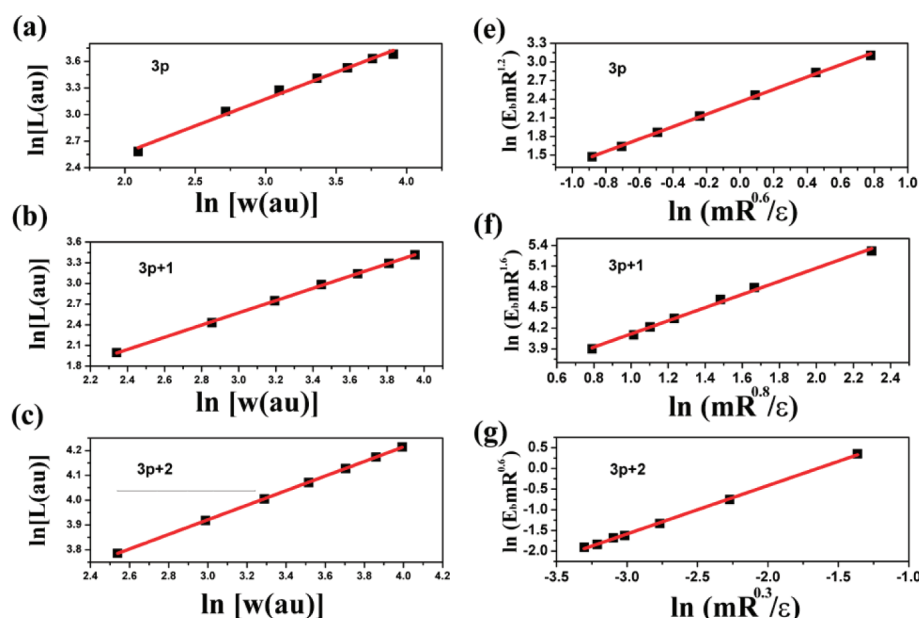


Figure 4. (a)–(c) Scaling relation between size of exciton (L) and the width (w). (d)–(e) Scaling relation between $E_b m w^{2\xi}$ and $m w^\xi / \epsilon$, where ξ is equal to 0.6, 0.8, and 0.3 for $3p$, $3p+1$, and $3p+2$ families, respectively. All the data are presented in logarithmic scale.

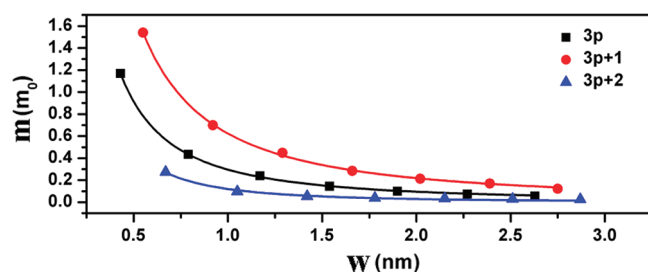


Figure 5. Scaling between the reduced mass (m) and the width (w) of the AGNRs. Here the reduced mass is defined as $m_e m_h / (m_e + m_h)$ in the unit of free electron mass, m_0 . The points are the raw data, and the lines are fitted to the formula: $m = A_m(w)^\tau$.

width increases. The detail dependence of the reduced mass of CNTs is inversely proportional to its diameter.⁴¹ The deviation of τ values from -1 is no surprise for AGNRs considering their zero curvature in geometry. We then obtain the following relationship by substituting w with $m^{1/\tau}$ into eq 4,

$$E_b = A_j m^\beta \epsilon^{-\alpha} \quad (6)$$

by defining m^β equals $m^{\alpha-1+(\alpha-2)\xi/\tau}$. The values of β are 0.35, 0.50, and 0.32 for $3p$, $3p+1$, and $3p+2$ family, respectively, as shown in Table 1. The positive values of β indicate that the binding energy increases as the reduced mass gets larger. More importantly, the change of the mass for the same family of AGNRs determines the scaling behavior of binding energy. Clearly the large deviation of β from unity breaks the usual linear correlation between binding energy and reduced mass deduced from the Rydberg approximation for the strong screening limit in the bulk form.⁴²

Despite the reported observation on the correlation between exciton binding energy and the size of CNTs,^{43,44} the explicit expression is still missing. Thus, it is highly desirable to express exciton binding energy as a function of the width of AGNRs.

Table 1. All the Exponents of the Scaling Formulas of Excitons in AGNRs^a

	ξ	τ	α	β	γ	δ
$3p$	0.60	-1.30	0.98	0.35	-0.60	-1.00
$3p+1$	0.80	-1.20	1.00	0.50	-0.73	-0.91
$3p+2$	0.30	-2.00	1.16	0.32	-0.55	-1.80

^a L is the size of exciton, w is the length of width of the AGNRs, E_b is the exciton binding energy, and m is the reduced effective mass. Exponents, i.e., ξ , τ , α , β , and γ , are fitting parameters in the scaling formulas, i.e., $L = A_w w^\xi$, $m = A_m w^\tau$, $E_b = A_p w^{(\alpha-2)\xi} m^{\alpha-1} \epsilon^{-\alpha}$, $E_b = A_j m^\beta \epsilon^{-\alpha}$, and $E_b = A_k w^\gamma \epsilon^{-\alpha}$. δ is defined as γ/ξ , which is the exponent in $E_b = A_L L^\delta$.

Their correlation is represented in the following equation by substituting m in eq 4 based on eq 5,

$$E_b = A_k w^\gamma \epsilon^{-\alpha} \quad (7)$$

by defining w^γ equals $w^{(\alpha-2)\xi+(\alpha-1)\tau}$. We fit the raw data by eq 7 as presented in Figure 6. Although there exists some deviation in the distribution of γ values due to the family effect, it is remarkable to observe that the fitted values of γ are distributed near -0.6 (see Table 1 for details), which originates from the delicate interplay of the correlation among width, exciton size, and reduce mass. Coincidentally, the same value was reported by Pedersen for the binding energy dependence on effective CNT radius.⁴⁵ However, the CNT radius used there was in the unit of the effective Bohr radius, which is proportional with m/ϵ^2 . Thus, the reported exponent there was not the direct scaling between binding energy and CNT radius. In fact, the exponent is approximately -1 when considering that the reduced mass scales linearly with CNT radius.⁴³ For AGNRs, the exponent in the power law turns out to be around -0.6 (and the exact family dependent values are listed in Table 1) as presented in eq 7, which is particularly useful to obtain the binding energy directly from the width of AGNRs.

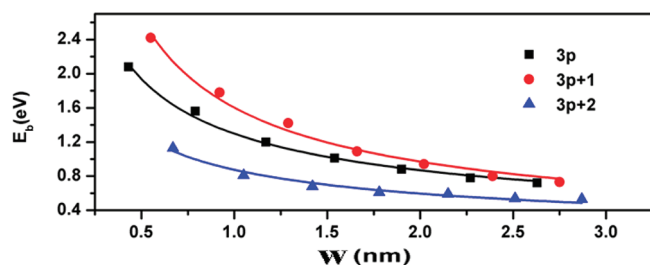


Figure 6. Scaling relation between the binding energy (E_b) and the width of AGNRs. The points are the raw data, and the lines are fitted to the formula $E_b = A_k w^\gamma e^{-\alpha}$.

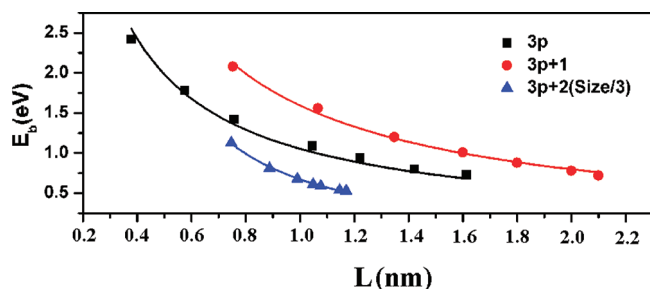


Figure 7. Scaling behavior between the binding energy (E_b) and the size (L) of the exciton. The points are raw data, and the lines are drawn with $E_b = A_L L^\delta$, where the values of δ are derived by γ/ξ in Table 1. The sizes of excitons in the $3p+2$ family are decreased to $1/3$ for clarify.

Finally, this family dependent relationship of the exciton size can be connected with the exciton binding energy as well.

$$E_b = A_L L^{[(\xi + \tau)\alpha - (2\xi + \tau)]/\xi} e^{-\alpha} = A_L L^\delta e^{-\alpha} \quad (8)$$

where δ equals $[(\xi + \tau)\alpha - (2\xi + \tau)]/\xi$. Figure 7 shows the scaling plot for the binding energy and the size of exciton. The size of the exciton is closely related to the exciton binding energy; for the families $3p$ and $3p+1$, which have medium binding energies, the size is below 5 nm, whereas for the $3p+2$ family, due to the low binding energy, a much larger size is expected, which is different from that of the other two families. The values of δ for both $3p$ and $3p+1$ are very close to -1 . For CNT, the binding energy scales approximately as R^{-1} , as discussed above. Considering the linear relationship between exciton size and CNT radius,²³ we anticipate that the exciton binding energy is approximately inverse proportional to the exciton size of the CNT. Thus, the excitons of the $3p$ and $3p+1$ families of AGNRs and CNTs have similar characters in this aspect. However, the $3p+2$ family of AGNRs has one very different value of δ , i.e., -1.8 , which is about 2 times larger than those of the other families of AGNRs and CNTs. Due to the curvature effect, the CNT band gap is larger than that of the corresponding AGNR when one excludes very small metallic CNTs caused by mixing σ and π bands. Therefore, the screening is expected to be notably enhanced in the $3p+2$ family of AGNRs, so that the exciton binding energy drops more rapidly as the exciton size increases.

CONCLUSIONS

We perform first principles studies on the optical properties of the AGNRs and develop comprehensive power-law scaling

formulas of the band gaps, exciton's reduced mass, binding energy, and size. The intrinsic zero curvature of AGNRs is manifested by the family dependent exponent as compared to the single exponent in SWCNTs, and the absent "family spreading" of optical transition energies in the smaller width region in the Kataura plots of AGNRs in sharp contrast to that in SWCNTs. In particular, the scaling formula between exciton binding strength and the geometric parameter of AGNRs is explicitly established.

ASSOCIATED CONTENT

S Supporting Information. Band gaps computed by local density approximation without and with GW correction together with their scaling behavior with AGNR's width. All the band gaps, optical transition energy, exciton binding energy, and reduced mass of AGNRs. This material is available free of charge via the Internet at <http://pubs.acs.org>.

AUTHOR INFORMATION

Corresponding Author

*E-mail: hbsu@ntu.edu.sg.

ACKNOWLEDGMENT

We are grateful for the interesting discussions with T. Ando and H. Ågren. The advice from Claudia Ambrosch-Draxl is particularly instructive. Work at NTU was supported in part by a MOE AcRF Tier-1 grant (grant no. M52070060) and A*STAR SERC grant (grant no. M47070020).

REFERENCES

- (1) Novoselov, K. S.; Geim, A. K.; Morozov, S. V.; Jiang, D.; Zhang, Y.; Dubonos, S. V.; Grigorieva, I. V.; Firsov, A. A. *Science* **2004**, *306*, 666–669.
- (2) Geim, A. K. *Science* **2009**, *324*, 1530–1534.
- (3) Castro Neto, A. H.; Guinea, F.; Peres, N. M. R.; Novoselov, K. S.; Geim, A. K. *Rev. Mod. Phys.* **2009**, *81*, 109–162.
- (4) Novoselov, K. S.; Geim, A. K.; Morozov, S. V.; Jiang, D.; Katsnelson, M. I.; Grigorieva, I. V.; Dubonos, S. V.; Firsov, A. A. *Nature* **2005**, *438*, 197–200.
- (5) Zhang, Y. B.; Tan, Y. W.; Stormer, H. L.; Kim, P. *Nature* **2005**, *438*, 201–204.
- (6) Du, X.; Skachko, I.; Duerr, F.; Luican, A.; Andrei, E. Y. *Nature* **2009**, *462*, 192–195.
- (7) Bolotin, K. I.; Ghahari, F.; Shulman, M. D.; Stormer, H. L.; Kim, P. *Nature* **2009**, *462*, 196–199.
- (8) Lin, Y. M.; Dimitrakopoulos, C.; Jenkins, K. A.; Farmer, D. B.; Chiu, H. Y.; Grill, A.; Avouris, P. *Science* **2010**, *327*, 662–662.
- (9) Son, Y.-W.; Cohen, M. L.; Louie, S. G. *Phys. Rev. Lett.* **2006**, *97*, 216803.
- (10) Yang, L.; Park, C. H.; Son, Y. W.; Cohen, M. L.; Louie, S. G. *Phys. Rev. Lett.* **2007**, *99*, 186801.
- (11) Wang, Z. F.; Li, Q. X.; Zheng, H. X.; Ren, H.; Su, H. B.; Shi, Q. W.; Chen, J. *Phys. Rev. B* **2007**, *75*, 113406.
- (12) Barone, V.; Hod, O.; Scuseria, G. E. *Nano Lett.* **2006**, *6*, 2748–2754.
- (13) Han, M. Y.; Ozyilmaz, B.; Zhang, Y. B.; Kim, P. *Phys. Rev. Lett.* **2007**, *98*, 206805.
- (14) Ozyilmaz, B.; Jarillo-Herrero, P.; Efetov, D.; Kim, P. *Appl. Phys. Lett.* **2007**, *91*, 192107.
- (15) Kosynkin, D. V.; Higginbotham, A. L.; Sinitskii, A.; Lomeda, J. R.; Dimiev, A.; Price, B. K.; Tour, J. M. *Nature* **2009**, *458*, 872–876.

- (16) Jiao, L. Y.; Zhang, L.; Wang, X. R.; Diankov, G.; Dai, H. J. *Nature* **2009**, *458*, 877–880.
- (17) Bai, J. W.; Duan, X. F.; Huang, Y. *Nano Lett.* **2009**, *9*, 2083–2087.
- (18) O'Connell, M. J.; Bachilo, S. M.; Huffman, C. B.; Moore, V. C.; Strano, M. S.; Haroz, E. H.; Rialon, K. L.; Boul, P. J.; Noon, W. H.; Kittrell, C.; Ma, J. P.; Hauge, R. H.; Weisman, R. B.; Smalley, R. E. *Science* **2002**, *297*, 593–596.
- (19) Bachilo, S. M.; Strano, M. S.; Kittrell, C.; Hauge, R. H.; Smalley, R. E.; Weisman, R. B. *Science* **2002**, *298*, 2361–2366.
- (20) Spataru, C. D.; Ismail-Beigi, S.; Benedict, L. X.; Louie, S. G. *Phys. Rev. Lett.* **2004**, *92*, 077402.
- (21) Samsonidze, G. G.; Saito, R.; Kobayashi, N.; Gruneis, A.; Jiang, J.; Jorio, A.; Chou, S. G.; Dresselhaus, G.; Dresselhaus, M. S. *Appl. Phys. Lett.* **2004**, *85*, 5703–5705.
- (22) Spataru, C. D.; Ismail-Beigi, S.; Capaz, R. B.; Louie, S. G. *Phys. Rev. Lett.* **2005**, *95*, 247402.
- (23) Perebeinos, V.; Tersoff, J.; Avouris, P. *Phys. Rev. Lett.* **2004**, *92*, 257402.
- (24) Onida, G.; Reining, L.; Rubio, A. *Rev. Mod. Phys.* **2002**, *74*, 601–659.
- (25) Giannozzi, P.; Baroni, S.; Bonini, N.; Calandra, M.; Car, R.; Cavazzoni, C.; Ceresoli, D.; Chiarotti, G. L.; Cococcioni, M.; Dabo, I.; Dal Corso, A.; de Gironcoli, S.; Fabris, S.; Fratesi, G.; Gebauer, R.; Gerstmann, U.; Gougoussis, C.; Kokalj, A.; Lazzeri, M.; Martin-Samos, L.; Marzari, N.; Mauri, F.; Mazzarello, R.; Paolini, S.; Pasquarello, A.; Paulatto, L.; Sbraccia, C.; Scandolo, S.; Sclauzero, G.; Seitsonen, A. P.; Smogunov, A.; Umari, P.; Wentzcovitch, R. M. *J. Phys.-Condens. Matter* **2009**, *21*, 395502.
- (26) Godby, R. W.; Needs, R. J. *Phys. Rev. Lett.* **1989**, *62*, 1169.
- (27) Rohlfing, M.; Louie, S. G. *Phys. Rev. B* **2000**, *62*, 4927.
- (28) Ismail-Beigi, S. *Phys. Rev. B* **2006**, *73*, 233103.
- (29) Rozzi, C. A.; Varsano, D.; Marini, A.; Gross, E. K. U.; Rubio, A. *Phys. Rev. B* **2006**, *73*, 205119.
- (30) Marini, A.; Hogan, C.; Gruning, M.; Varsano, D. *Comput. Phys. Commun.* **2009**, *180*, 1392.
- (31) Marinopoulos, A. G.; Reining, L.; Rubio, A.; Vast, N. *Phys. Rev. Lett.* **2003**, *91*, 046402.
- (32) Ajiki, H.; Ando, T. *Physica (Amsterdam)* **1994**, *201B*, 349.
- (33) Prezzi, D.; Varsano, D.; Ruini, A.; Marini, A.; Molinari, E. *Phys. Rev. B* **2008**, *77*, 41404.
- (34) Yang, L.; Cohen, M. L.; Louie, S. G. *Nano Lett.* **2007**, *7*, 3112–3115.
- (35) Zhu, X.; Su, H. B. *J. Phys. Chem. C* **2010**, *114*, 17257–17262.
- (36) Hybertsen, M. S.; Louie, S. G. *Phys. Rev. B* **1986**, *34*, 5390.
- (37) Kataura, H.; Kumazawa, Y.; Maniwa, Y.; Umez, I.; Suzuki, S.; Ohtsuka, Y.; Achiba, Y. *Synth. Met.* **1999**, *103*, 2555.
- (38) Wang, F.; Cho, D. J.; Kessler, B.; Deslippe, J.; Schuck, P. J.; Louie, S. G.; Zettl, A.; Heinz, T. F.; Shen, Y. R. *Phys. Rev. Lett.* **2004**, *99*, 227401.
- (39) Kane, C. L.; Mele, E. J. *Phys. Rev. Lett.* **2003**, *90*, 207401.
- (40) Blase, X.; Benedict, L. X.; Shirley, E. L.; Louie, S. G. *Phys. Rev. Lett.* **1994**, *72*, 1878.
- (41) Ando, T. *J. Phys. Soc. Jpn.* **1997**, *66*, 1066–1073.
- (42) Michael, P. Marder. *Condensed Matter Physics*; Wiley-Interscience: New York, 2000;
- (43) Dukovic, G.; Wang, F.; Song, D.; Sfeir, M. Y.; Heinz, T. F.; Brus, L. E. *Nano Lett.* **2005**, *5*, 2314–2318.
- (44) Hummer, K.; Ambrosch-Draxl, C. *Phys. Rev. B* **2005**, *71*, 081202.
- (45) Pedersen, T. G. *Phys. Rev. B* **2003**, *67*, 073401.